Mid-infrared photonic crystal waveguides in silicon

Christian Reimer,[1,2,*] Milos Nedeljkovic,[3] David J. M. Stothard,[2] Matthieu O. S. Esnault,[2] Christopher Reardon,[2] Liam O'Faolain,[2] Malcolm Dunn,[2] Goran Z. Mashanovich,[3] and Thomas F. Krauss[2]

[1]*INRS-EMT, 1650 Boul. Lionel-Boulet, Varennes, Québec J3X 1S2, Canada*
[2]*SUPA, School of Physics and Astronomy, University of St Andrews, Fife KY16 9SS, UK*
[3]*Optoelectronics Research Center, University of Southampton, Southampton SO17 1BJ, UK*
[*]*reimer@emt.inrs.ca*

Abstract: We demonstrate the design, fabrication and characterization of mid-infrared photonic crystal waveguides on a silicon-on-insulator platform, showing guided modes in the wavelength regime between 2.9 and 3.9 μm. The characterization is performed with a proprietary intra-cavity Optical Parametric Oscillator in a free space optical setup and with a fibre coupled setup using a commercial Quantum Cascade Laser. We discuss the use of an integrated Mach-Zehnder interferometer for dispersion measurements and report a measured group velocity of up to a value of n_g = 12, and determine the propagation loss to be 20 dB/cm.

OCIS codes: (130.5296) Photonic crystal waveguides; (230.5298) Photonic crystals; (350.4238) Nanophotonics and photonic crystals.

References and links

1. R. Soref, "Mid-infrared photonics in silicon and germanium," Nat. Photonics **4**(8), 495–497 (2010).
2. M. M. Milošević, M. Nedeljkovic, T. M. Ben Masaud, E. Jaberansary, H. M. H. Chong, N. G. Emerson, G. T. Reed, and G. Z. Mashanovich, "Silicon waveguides and devices for the mid-infrared," Appl. Phys. Lett. **101**(12), 121105 (2012).
3. X. Liu, R. M. Osgood, Jr., Y. A. Vlasov, and W. M. J. Green, "Mid-infrared optical parametric amplifier using silicon nanophotonic waveguides," Nat. Photonics **4**(8), 557–560 (2010).
4. J. Li, L. O'Faolain, I. H. Rey, and T. F. Krauss, "Four-wave mixing in photonic crystal waveguides: slow light enhancement and limitations," Opt. Express **19**(5), 4458–4463 (2011).
5. B. Corcoran, C. Monat, C. Grillet, D. J. Moss, B. J. Eggleton, T. P. White, L. O'Faolain, and T. F. Krauss, "Green light emission in silicon through slow-light enhanced third harmonic generation in photonic crystal waveguides," Nat. Photonics **3**(4), 206–210 (2009).
6. R. Shankar, R. Leijssen, I. Bulu, and M. Lončar, "Mid-infrared photonic crystal cavities in silicon," Opt. Express **19**(6), 5579–5586 (2011).
7. R. Shankar, I. Bulu, R. Leijssen, and M. Lončar, "Study of thermally-induced optical bistability and the role of surface treatments in Si-based mid-infrared photonic crystal cavities," Opt. Express **19**(24), 24828–24837 (2011).
8. C. Reimer, M. Nedeljkovic, D. J. M. Stothard, G. Z. Mashanovich, and T. F. Krauss, "Mid-infrared photonic crystal waveguides in SOI," in *Proceedings of IEEE International Conference of Group IV Photonics (GFP)*, ed. (Conference Publications, San Diego, Calif., 2012), pp 12–14.
9. M. I. T. Photonic Bands, http://ab-initio.mit.edu/wiki/index.php/MIT_Photonic_Bands
10. L. O'Faolain, S. A. Schulz, D. M. Beggs, T. P. White, M. Spasenović, L. Kuipers, F. Morichetti, A. Melloni, S. Mazoyer, J. P. Hugonin, P. Lalanne, and T. F. Krauss, "Loss engineered slow light waveguides," Opt. Express **18**(26), 27627–27638 (2010).
11. J. P. Hugonin, P. Lalanne, T. P. White, and T. F. Krauss, "Coupling into slow-mode photonic crystal waveguides," Opt. Lett. **32**(18), 2638–2640 (2007).
12. C. P. Reardon, I. H. Rey, K. Welna, L. O'Faolain, and T. F. Krauss, "Fabrication and characterisation of photonic crystal slow light waveguides and cavities," J. Vis. Exp. (69): e50216 (2012), doi:10.3791/50216, http://www.jove.com/video/50216/fabrication-characterisation-photonic-crystal-slow-light-waveguides?status=a52222k.
13. G. Z. Mashanovich, M. M. Milošević, M. Nedeljkovic, N. Owens, B. Xiong, E. J. Teo, and Y. Hu, "Low loss silicon waveguides for the mid-infrared," Opt. Express **19**(8), 7112–7119 (2011).

#179013 - $15.00 USD Received 1 Nov 2012; revised 8 Dec 2012; accepted 9 Dec 2012; published 18 Dec 2012

14. D. J. M. Stothard, M. Ebrahimzadeh, and M. H. Dunn, "Low-pump-threshold continuous-wave singly resonant optical parametric oscillator," Opt. Lett. **23**(24), 1895–1897 (1998).
15. D. J. M. Stothard, C. F. Rae, and M. H. Dunn, "An intracavity optical parametric oscillator with very high repetition rate and broad tunability based upon room temperature periodically-poled MgO:LiNbO3 with fanned grating design," IEEE J. Quantum Electron. **45**(3), 256–263 (2009).
16. E. Kuramochi, M. Notomi, S. Hughes, A. Shinya, T. Watanabe, and L. Ramunno, "Disorderinduced scattering loss of line-defect waveguides in photonic crystal slabs," Phys. Rev. B **72**(16), 161318 (2005).
17. E. Dulkeith, F. Xia, L. Schares, W. M. J. Green, and Y. A. Vlasov, "Group index and group velocity dispersion in silicon-on-insulator photonic wires," Opt. Express **14**(9), 3853–3863 (2006).
18. L. O'Faolain, X. Yuan, D. McIntyre, S. Thoms, H. Chong, R. M. De La Rue, and T. F. Krauss, "Low-loss propagation in photonic crystal waveguides," Electron. Lett. **42**(25), 1454–1455 (2006).
19. M. Notomi, T. Tanabe, A. Shinya, E. Kuramochi, H. Taniyama, S. Mitsugi, and M. Morita, "Nonlinear and adiabatic control of high-Q photonic crystal nanocavities," Opt. Express **15**(26), 17458–17481 (2007).
20. S. L. Portalupi, M. Galli, M. Belotti, L. C. Andreani, T. F. Krauss, and L. O'Faolain, "Deliberate versus intrinsic disorder in photonic crystal nanocavities investigated by resonant light scattering," Phys. Rev. B **84**(4), 045423 (2011).
21. B. Wang, S. Mazoyer, J. P. Hugonin, and P. Lalanne, "Backscattering in monomode periodic waveguides," Phys. Rev. B **78**(24), 245108 (2008).

1. Introduction

There is growing interest in the mid-infrared (mid-IR) wavelength range (2-20μm) due to its promising applications in thermal imaging, biological and gas sensing, free space communication and nonlinear optics. As proposed by Soref [1], silicon is a very interesting material for the mid-IR wavelength range due to its transparency window between 1.1 and 8.5 μm. Since silicon dioxide is also transparent up to around 3.6 μm [1], silicon-on-insulator (SOI) forms a very promising platform for mid-IR integrated photonics [2]. It has been shown that nonlinear effects such as four-wave-mixing (FWM) or parametric amplification can also be enhanced by moving into the wavelength regime above the two-photon absorption bandedge of silicon, i.e. >2.2 μm [3]. Photonic crystal (PhC) waveguides, especially slow light PhC waveguides, have already shown enhanced nonlinear effects such as FWM [4] and third harmonic generation (THG) [5], but are typically limited by linear and nonlinear losses. By extending the wavelength of operation into the mid-IR regime, above the two-photon absorption bandedge, nonlinear losses can be almost eliminated. Furthermore, linear losses are expected to be reduced in mid-IR PhC waveguides once the same roughness values can be achieved as in the near-infrared (near-IR). Mid-IR PhC waveguides therefore form a very promising platform for nonlinear optical applications, because they can combine slow-light enhancement with potentially low linear propagation loss and strongly reduced nonlinear losses. Mid-IR PhC cavities have already been demonstrated between 4.4 and 4.6 μm in SOI [6, 7]. To date we are not aware of any demonstration of PhC waveguides in the mid-IR wavelength range in SOI. We recently presented the first transmission through PhC waveguides for mid-IR wavelengths [8], and here present a full characterization of the first mid-IR PhC waveguides in SOI including transmission, group index and loss measurements. We note that fabrication and characterization do not simply scale up from the processes now familiar at 1.55 μm, which explains some of the difficulties. As part of the characterization, we introduce the use of a proprietary intra-cavity Optical Parametric Oscillator (OPO) as a characterization tool in addition to a more commonly used commercial Quantum Cascade Laser (QCL). Furthermore, we describe the technique of measuring the group index with a lithographically integrated Mach-Zehnder interferometer, and present first propagation loss values determined by the cut-back technique.

2. Design and fabrication

To demonstrate mid-IR PhC waveguides, we chose the well-known W1 design, which consists of a two-dimensional hexagonal PhC lattice of air holes in a silicon slab with one row of holes removed (Fig. 1) and vertical confinement provided by total internal reflection.

#179013 - $15.00 USD Received 1 Nov 2012; revised 8 Dec 2012; accepted 9 Dec 2012; published 18 Dec 2012

Simulations were performed using the MIT Photonic Bands package (MPB) [9] and the waveguide design script developed by our group and outlined in [10].

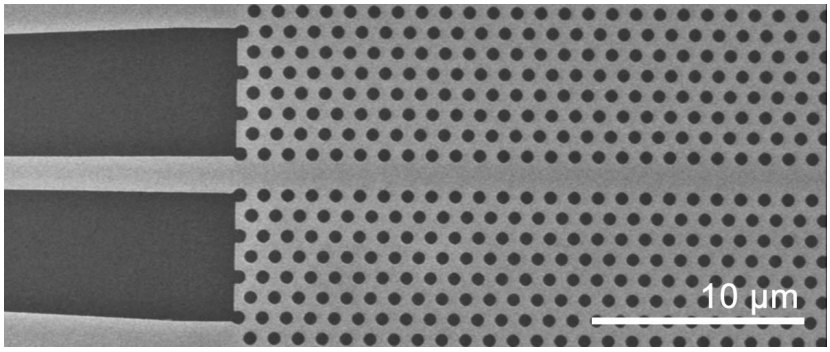

Fig. 1. SEM image of a mid-IR W1 PhC and access waveguide.

A number of different W1 PhC waveguides with varying lattice periods between a = 1040 −1120 nm and hole radii r/a = 0.26-0.28 were fabricated, targeting guided modes between 2.9 µm and 3.9 µm. The top view of a typical structure is shown in Fig. 1. Light is coupled into an access waveguide, which is etched on the sample together with the PhC waveguide. The coupling efficiency between access and PhC waveguide is very high for low group indices, but typically decreases for higher group indices. This poor coupling efficiency can be addressed by adding a short coupling region, where the PhC is slightly stretched parallel to the waveguide, thereby achieving coupling efficiencies above 90% in the slow light regime of the PhC waveguide with group indices above 100 [11]. Such a coupling region becomes important when using slow-light dispersion engineered waveguides [10] but is not used in our W1 PhC waveguide demonstration. The devices are fabricated on an SOI wafer (SOITEC Inc.) consisting of a 500 nm thick silicon device layer on a 3 µm thick silicon dioxide layer on a silicon substrate. A 1 µm thick layer of positive electron-beam resist ZEP-520A (Zeon Corp) is deposited by spin-coating two layers of ZEP at 1600 rpm, each layer baked at 180°C for 10 minutes. The patterns are defined using a RAITH Elphy Plus/LEO1530 electron-beam lithography system at 30kV and transferred into the silicon layer directly using low power (19 W), low DC bias (–210 V) reactive ion etching with a mixture of SF_6 and CHF_3 gases (1:1 gas ratio). After etching, the remaining ZEP-520A is removed, a layer of Microposit S1818 G2 photoresist is deposited and windows are opened in the photoresist above the PhC regions via UV lithography. Using buffered hydrofluoric acid (1:6 ratio of HF to NH_4F), the silicon dioxide is selectively removed below the PhC areas. The fabricated devices are then cleaned using a Piranha solution (1:3 ratio of H_2O_2 to H_2SO_4) to remove any remaining resist, and the access waveguides are cleaved in order to enable end-fire coupling [12].

3. Characterisation

Working in the mid-IR wavelength regime has proved challenging due to the limitations of available equipment. The largest issue is the alignment of the beam for coupling light in and out of the sample, as mid-IR viewing cards, cameras, and optical components are not as well developed as those used in the 1.5 µm regime. Here, we used a commercially available tuneable quantum cascade laser (QCL, Daylight Solutions Inc.) with a tuning range between 3.7 and 3.9 µm, with up to 150mW CW output power and a tuning step size of down to 10 pm, coupled into a single-mode fluoride fibre with a 9 µm core [13]. This approach allows the fibres to be visibly aligned, although a relatively high insertion loss into the fibers of around 15 dB and further insertion losses in the region of 10 dB/facet from the fiber to the sample must be tolerated, as lensed fibres are not available. Alternatively, we introduced a free-space setup using a proprietary OPO. The OPO was designed and built at the University of St

#179013 - $15.00 USD Received 1 Nov 2012; revised 8 Dec 2012; accepted 9 Dec 2012; published 18 Dec 2012

Andrews and emits near- and mid-IR light collinearly (Fig. 2). The collinearity of the near- and mid-IR wavelengths enables sample alignment with standard near-IR viewing cards and cameras in a free-space setup. The free-space set-up employs CaF_2 lenses and ZnSe microscope objectives that can operate at both near- and mid-IR, and a near-IR Ge detector together with a mid-IR PbSe detector are used. As the near-IR emission is closely correlated with the mid-IR signal, it is used for monitoring and wavelength control. The OPO features a fan-grated magnesium oxide doped periodically poled lithium niobate (MgO:PPLN) crystal with a grating period of 29.5-32.5 µm, which allows for a wide tuning range from 2.9 µm to 3.7 µm. The nonlinear crystal was mounted in a computer-controlled, stepper motor actuated translation stage for automated tuning of the down-converted signal and idler waves. To reduce the threshold power and increase the stability, an intra-cavity OPO design is used, where the MgO:PPLN crystal is placed directly inside the pump laser cavity [14]. The device can operate in pulsed mode via an intra-cavity acousto-optic Q-switch, which achieves a pulse repetition rate of ≈300 kHz [15]. The 10 µm translation resolution of the MgO:PPLN crystal yields an OPO tuning step size of ≈1 nm over the full range of 2.9 to 3.7 µm. The CW linewidth of the OPO is $\Delta\lambda \approx 10$ pm, but due to jitter caused by Q-switching–related instabilities and broadened parametric gain, the useful effective Q-switched linewidth is in the order of $\Delta\lambda_{eff} \approx 3$ nm. The OPO achieves an average output power between 120 and 180 mW resulting in a Q-switched peak power of ≈50-70 W.

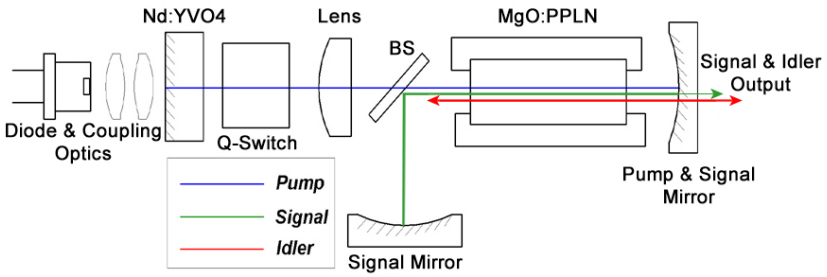

Fig. 2. Schematic of the cavity design of the custom made intra-cavity OPO.

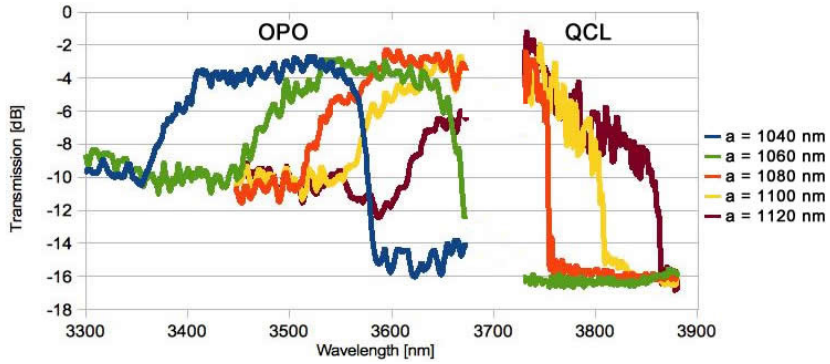

Fig. 3. Measured transmission through photonic crystal waveguides with lattice periods between a = 1040 – 1120 nm, measured with the free-space OPO, as well as the fibre couple QCL setup. Clear cut-offs are visible, showing good agreement with simulations [8].

We characterised our 200 µm long W1 PhC waveguides using the both optical setups and show the combined results in Fig. 3, normalized to an access waveguide [8]. As expected, clear short and long wavelength cut-offs are apparent that correspond to the position of the light line and the PhC bandgap, respectively. We note a small (4% in wavelength) blueshift between the measurements and the simulations, which is consistent on both setups, thus pointing to either an imprecise refractive index used in the simulations, or, more likely,

#179013 - $15.00 USD Received 1 Nov 2012; revised 8 Dec 2012; accepted 9 Dec 2012; published 18 Dec 2012

variations in the slab thickness of the SOI. Losses on the short wavelength side of the central passband are lower than on the long wavelength side, which is due to the waveguides operating above the light line; above the light line, propagation is possible, although the mode can leak to the continuum, whereas beyond the cut-off on the long wavelength side, no propagation is possible at all [16]. The large tuning range of the OPO allows the mapping of transmission properties across the entire photonic bandgap (Fig. 4) [8]. The corresponding cut-off positions are highlighted in the simulated band diagram, showing good agreement with the measurement. In particular, we measured cut-off positions at 3040, 3515 and 3690 nm in a PhC waveguide with a = 1060 nm and r/a = 0.285 and simulated values of 3038, 3509 and 3714 nm, respectively after correcting for the 4% blueshift.

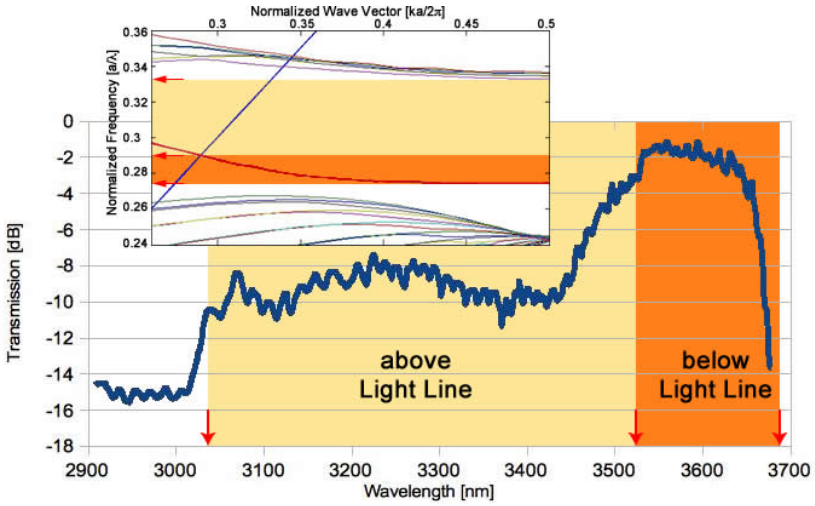

Fig. 4. Transmission measurement of a PhC waveguide with lattice period a = 1060 nm. The full tuning range of the OPO is exploited in order to measure the transmission above and below the light line. Three separate cut-offs are measured, corresponding to the beginning of guided modes, the light line and the PhC bandgap, respectively. The inset shows the simulated band diagram of the PhC waveguide, where the cut-off positions and guided modes above and below the light line are highlighted [8].

An important and characteristic property of PhC waveguides is the dispersion of the guided mode, with the corresponding group index increasing towards the band-edge at $a/\lambda \approx 0.275$ (Fig. 4, inset). In the near-IR, the group index is commonly measured by placing the PhC waveguide inside one arm of an interferometer and measuring the interference fringes with an optical spectrum analyser (OSA) [12]. Building a mid-IR interferometer, however, is very challenging due to technological limitations in beam splitters and especially in the required alignment and calibration. Furthermore, no OSAs exist for the wavelength range used here, making the task of measuring the dispersion and group index more difficult. To solve these technological issues, we lithographically integrate an unbalanced Mach-Zehnder interferometer (MZI) onto the chip (Fig. 5(a)) and scan the wavelength in order to measure the interference pattern without the need for an OSA or an external interferometer. The MZI is formed by utilizing two single mode 50:50 y-splitters (Fig. 5(c)), and placing a PhC waveguide in one arm of the MZI (Fig. 5(b)). In order to map the group indices, we measure the transmission through the MZI across the full OPO tuning range, where an interference pattern only appears in the transmission band of the PhC, since otherwise light only travels through one arm of the MZI without interference. The interference pattern of a wavelength scan through an integrated MZI is shown in the inset in Fig. 6. Here a 200 µm long PhC waveguide with lattice period a = 1040 nm is placed in one arm and the data is normalized to a transmission of 0.5 outside the interference region. Since the phase difference between

#179013 - $15.00 USD Received 1 Nov 2012; revised 8 Dec 2012; accepted 9 Dec 2012; published 18 Dec 2012

adjacent extrema is π, the group index can be extracted, which is given by: $n_g = (\lambda_{min} \cdot \lambda_{max})/(2 \cdot L \cdot \Delta\lambda)$, where $\lambda_{min}, \lambda_{max}$ are the positions of adjacent minima and maxima, $\Delta\lambda$ is the spectral difference between the extrema, and L the length of the PhC waveguide [17].

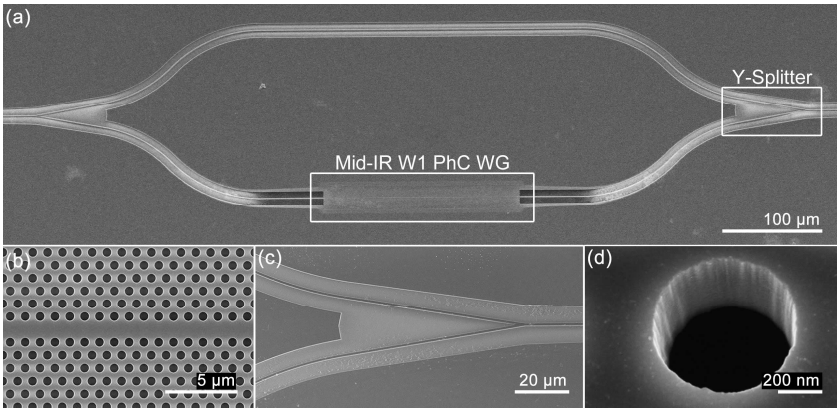

Fig. 5. SEM images of (a) an integrated unbalanced mid-IR MZI used to measure the group index of the PhC waveguides. The PhC waveguide (b) is placed in one arm of the MZI and two single-mode 50:50 y-splitters (c) are used to split into and recombine the two arms. A single hole of the PhC is shown in (d), showing relatively high sidewall roughness.

The measured group index values are plotted in Fig. 6, superimposed on the corresponding MPB bandstructure calculation, showing excellent agreement between measurements and simulation. Due to the limited effective linewidth of $\Delta\lambda \approx 3$nm, and the strong dispersion and losses of the waveguide in the high group index regime near the bandedge, we were not able to measure group indices higher than $n_g \approx 12$. We believe that higher values can be obtained, however, even with the large $\Delta\lambda_{eff}$ of the OPO, by operating in a "dispersion engineered" regime [10], where constant group indices over several nm linewidth can be achieved.

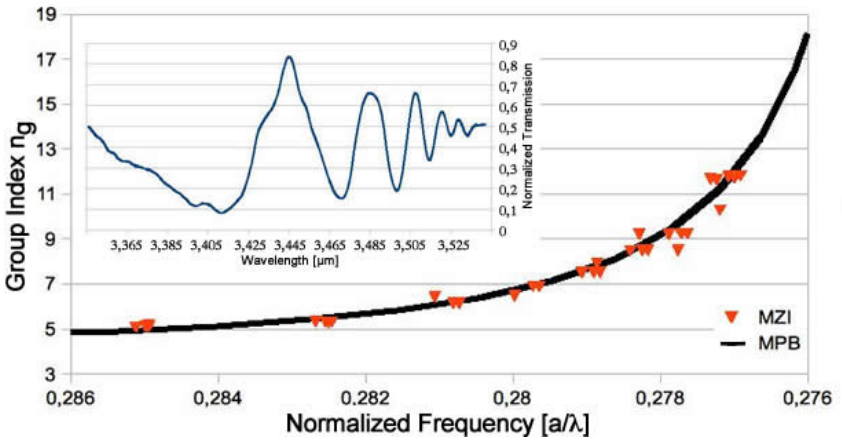

Fig. 6. Group indices measured using an integrated MZI (orange triangles), and simulated group index curve using the MPB package (black line). The normalized experimental interference pattern of a single wavelength scan is shown in the inset.

The propagation loss of the PhC waveguides is determined by the cut-back technique by measuring the transmission through twelve PhC waveguides with lattice period a = 1040 nm of lengths between 200 µm and 1 mm (Fig. 7). First measurements show a propagation loss of 20 +/- 2 dB/cm in the $n_g = 5$ ($\lambda = 3.4$ µm) regime of the guided mode below the light line.

#179013 - $15.00 USD Received 1 Nov 2012; revised 8 Dec 2012; accepted 9 Dec 2012; published 18 Dec 2012

This relatively high loss compared to near-IR PhC waveguides is due to higher roughness at the sidewalls of the PhC holes (Fig. 5(d)). The main challenge is to etch the thicker device layer of 500 nm with comparable roughness, to that already achieved in the 220 nm thick layers used for 1.5 μm operation. In the near-IR, propagation losses below 5 dB/cm [18] with a record of 2 dB/cm [19] have been achieved, and roughness values below 1 nm have been demonstrated [20]. Such low roughness is already close to the technological limit and further improvements require additional improvements in more loss-tolerant waveguide designs [10]. For the mid-IR, on the other hand, there is more room for improvement due to the larger feature sizes and not yet fully optimized fabrication techniques. Once the fabrication processes have been optimized for the thicker SOI, and similar roughness values of below 1 nm have been achieved, the propagation loss of mid-IR PhC waveguides is expected to be significantly lower than in the near-IR due to the larger ratio between wavelength and roughness. In particular, the loss is expected to scale as $(\sigma/\lambda)^2$ [21], with σ the root-mean-squared roughness. Hence, the loss measurements presented here only provide a first benchmark of the performance of mid-IR PhC waveguides in 500 nm thick SOI and loss values are expected to improve in due course.

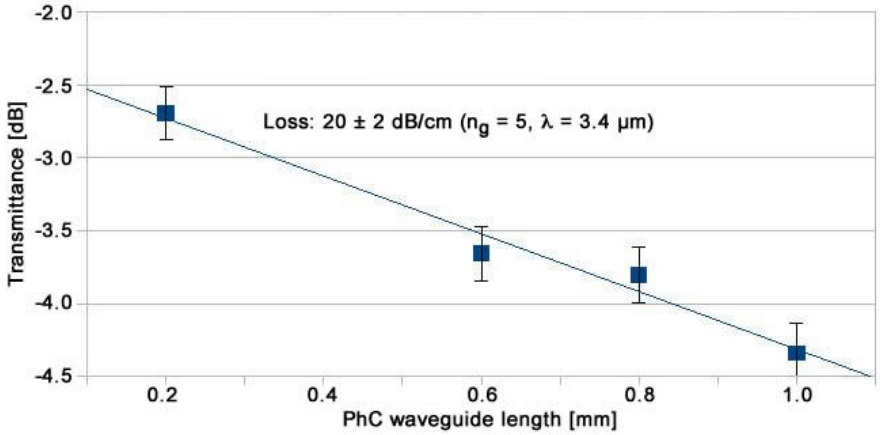

Fig. 7. Propagation loss measurement of mid-IR PhC W1 waveguide with lattice period a = 1040 nm, measured at group index ng = 5 at 3.4 μm wavelength. The loss was determined by measuring the transmission through twelve PhC waveguides, and by fitting a line through the normalized intensity as a function of waveguide length.

4. Conclusion

In conclusion, we have demonstrated the design, fabrication and characterization of photonic crystal waveguides in SOI for the mid-IR wavelength range between 2.9 and 3.9 μm. The waveguides were characterized using a commercial quantum cascade laser and a proprietary optical parametric oscillator, where both setups are designed to characterize mid-IR PhC waveguides without the need for expensive mid-IR cameras. The group index was measured using an integrated Mach-Zehnder Interferometer. The measurement was limited to a group index value of $n_g \approx 12$ by the relatively large effective linewidth of the OPO. This limitation can be addressed by using dispersion engineered slow light waveguides, which will allow access to much higher group index values and correspondingly will allow the observation of nonlinear effects. We also measured a propagation loss of 20 dB/cm in the fast light regime, which can be explained by the observed hole roughness caused by the difficulties in scaling up the fabrication processes. As the propagation loss is limited by roughness scattering and scales as $(\sigma/\lambda)^2$ [21], we ultimately expect a better loss performance at the longer mid-IR wavelengths than in the 1.5μm regime. For nonlinear application, less loss sensitive "dispersion engineered" waveguide designs can be utilized, which will offer lower losses at

#179013 - $15.00 USD Received 1 Nov 2012; revised 8 Dec 2012; accepted 9 Dec 2012; published 18 Dec 2012

higher group indices. As demonstrated in the near-IR, nonlinear losses play an important role when measuring nonlinear optical phenomena such as THG, where the conversion efficiency saturates already at low coupled input powers of 60 μW [5]. Without this saturation in the mid-IR, the converted optical power of THG will scale with the third power of the coupled pump [5], while scattering losses linearly reduce the effective pump power. We therefore expect high nonlinear conversion efficiencies in mid-IR PhC waveguides. Overall, it is clear that mid-IR PhC waveguides will form a very powerful platform for the investigation of nonlinear optical phenomena.

Acknowledgments

The authors acknowledge financial support from EPSRC through the "UK Silicon Photonics" and the "Structured Light" Programme Grants. G. Z. Mashanovich would like to acknowledge support by the Royal Society through his Royal Society Research Fellowship.

#179013 - $15.00 USD Received 1 Nov 2012; revised 8 Dec 2012; accepted 9 Dec 2012; published 18 Dec 2012